

Anisotropy of (partial) isothermal remanent magnetization:

DC-field-dependence and additivity

Andrea R. Biedermann<sup>1,2</sup>, Mike Jackson<sup>1</sup>, Dario Bilardello<sup>1</sup>, Joshua M. Feinberg<sup>1</sup>

<sup>1</sup> Institute for Rock Magnetism, University of Minnesota, Minneapolis, MN, USA

<sup>2</sup> Institute of Geological Sciences, University of Bern, Bern, Switzerland

Accepted date May 13<sup>th</sup>, 2019

Received date: May 10<sup>th</sup>, 2019

in original form date: March 11<sup>th</sup>, 2019

Address for correspondence:

Prof. Andrea R. Biedermann  
Institute of Geological Sciences  
University of Bern  
Baltzerstrasse 1+3  
3012 Bern  
Switzerland  
[andrea.regina.biedermann@gmail.com](mailto:andrea.regina.biedermann@gmail.com)  
Phone: +41 (0)31 631 8764

Abbreviated title:

A(p)IRM field-dependence and additivity

## Summary:

Anisotropy of isothermal remanent magnetization (AIRM) is useful for describing the fabrics of high-coercivity grains, or alternatively, the fabrics of all remanence-carrying grains in rocks with weak remanence. Comparisons between AIRM and other measures of magnetic fabric allow for description of mineral-specific or grain-size-dependent fabrics, and their relation to one another. Additionally, when the natural remanence of a rock is carried by high-coercivity minerals, it is essential to isolate the anisotropy of this grain fraction to correct paleodirectional and paleointensity data. AIRMs have been measured using a wide range of applied fields, from a few mT to several T. It has been shown that the degree and shape of AIRM can vary with the strength of the applied field, e.g. due to the contribution of separate grain subpopulations or due to field-dependent properties. To improve our understanding of these processes, we systematically investigate the variation of AIRM and the anisotropy of partial isothermal remanence (ApIRM) with applied field for a variety of rocks with different magnetic mineralogies. We also test the additivity of A(p)IRMs and provide a definition of their error limits. While A(p)IRM principal directions can be similar for a range of applied field strengths on the same specimen, the degree and shape of anisotropy often show systematic changes with the field over which the (p)IRM was applied. Also the data uncertainty varies with field window; typically, larger windows lead to better-defined principal directions. Therefore, the choice of an appropriate field window is crucial for successful anisotropy corrections in paleomagnetic studies. Due to relatively large deviations between AIRMs calculated by tensor addition and directly measured AIRMs, we recommend that the desired A(p)IRM be measured directly for anisotropy corrections.

**Keywords:**

Magnetic fabrics and anisotropy < GEOMAGNETISM and ELECTROMAGNETISM

Magnetic properties < COMPOSITION and PHYSICAL PROPERTIES

Rock and mineral magnetism < GEOMAGNETISM and ELECTROMAGNETISM

## 1. Introduction

Magnetic fabrics are a fast and efficient measure of mineral textures (Borradaile and Henry, 1997, Borradaile and Jackson, 2010, Hrouda, 1982, Tarling and Hrouda, 1993, Martín-Hernández *et al.*, 2004, Owens, 1974, Rochette *et al.*, 1992). Anisotropy of remanent magnetization, in particular, provides information on the preferred alignment of remanence-carrying grains, and can be used to correct paleodirectional and paleointensity data for the effects of anisotropic remanence acquisition (Jackson and Tauxe, 1991, Jackson, 1991, Stephenson *et al.*, 1986, Biedermann *et al.*, 2019). The anisotropy of anhysteretic remanent magnetization (AARM) is often chosen for these purposes, because it is considered the best room-temperature equivalent of a natural thermoremanent magnetization (Potter, 2004). However, AARM measurements target low- and intermediate-coercivity grains and are thus mainly applicable to samples whose remanence is carried by magnetite and its titanium-substituted equivalents. By contrast, the anisotropy of isothermal remanent magnetization (AIRM) targets also the high-coercivity remanence carriers that are not magnetized in the weak fields used during AARM measurements (Cox and Doell, 1967). For this reason, AIRM is preferentially used to correct paleomagnetic data in hematite-rich sediments or lunar rocks (Hodych and Buchan, 1994, McCall and Kodama, 2014, Bilardello and Kodama, 2009, Garrick-Bethell *et al.*, 2016, Tikoo *et al.*, 2012, Tamaki and Itoh, 2008, Stokking and Tauxe, 1990, Font

*et al.*, 2005). An additional advantage of AIRM is that isothermal remanences (IRMs) are stronger than anhysteretic remanences (ARMs). Therefore, IRMs imposed in low fields (e.g.,  $\leq 60$  mT) have been used to characterize the magnetite contribution to remanence anisotropy (Stephenson *et al.*, 1986, Kovacheva *et al.*, 2009, Bogue *et al.*, 1995, Cagnoli and Tarling, 1997, Raposo *et al.*, 2003, Tarling and Hrouda, 1993, Bascou *et al.*, 2002, di Capua, 2014). A survey of earlier AIRM research has shown that depending on the goal of a study, the anisotropy of isothermal remanence can be measured by applying fields between a few mT and 13 T in a number of specimen orientations (typically 3 or 9), or by measuring IRM acquisition curves along several directions. Most studies used pulse magnetizers to impart IRMs. Sometimes, specimens were demagnetized between magnetizing steps in different directions; however, this was not always possible, especially when the IRM fields were greater than the maximum demagnetizing alternating fields (AF) available. If a specimen saturates in the applied field, then demagnetization between directions is not necessary. Another approach to avoid problems of residual magnetization is using multiple specimens to define the anisotropy, which also avoids issues of thermochemical alteration (Bilardello, 2015). In summary, AIRM is preferred over AARM mainly in two cases: (1) when rocks are dominated by high-coercivity remanence carriers (Kodama and Dekkers, 2004), or (2) when a rock's remanence is near the sensitivity of one's rock magnetometers (Potter, 2004).

As a consequence of the different minerals it targets, when combined with other methods, AIRM can provide additional information on the nature of magnetic and mineral fabrics that could not be obtained from one method alone. For example, Lu and McCabe (1993) compared AARM and AIRM in carbonate rocks from the Nashville (Tennessee, USA) and the Jessamine (Kentucky, USA) domes, and found that their AARM reflects both a depositional and compaction fabric while the AIRM represents a later tectonic overprint. Henry and Daly (1983) and Hrouda (2002b) proposed that paramagnetic and ferromagnetic contributions to the magnetic fabrics can be separated based on a comparison between anisotropy of magnetic susceptibility (AMS) and AIRM (but see caveats in Hrouda *et al.* (2000)). More recent separation methods exploit the different field- and temperature-dependencies

of paramagnetic and ferromagnetic properties (Martín-Hernández and Ferré, 2007). Numerous studies have used combinations of AMS, AARM, AIRM and anisotropy of thermal remanence (ATRM) to better understand the carriers of magnetic fabrics, in aid of their interpretation (Tema, 2009, Raposo *et al.*, 2004, Bilardello and Jackson, 2014, Agro *et al.*, 2017, Lycka, 2017, Selkin *et al.*, 2000, Biedermann *et al.*, 2016, Borradaile and Dehls, 1993, Lawrence *et al.*, 2002).

While a comparison between AMS, AARM, ATRM and AIRM is useful for a first characterization of different carrier minerals and their fabrics, it is possible to separate different grain subpopulations even more deliberately. Subpopulations of remanence-carrying grains may define distinct fabrics for different grain sizes or compositions, resulting, for example, in AARMs and anisotropy of partial ARMs (ApARM) that vary with coercivity (Jackson *et al.*, 1989, Trindade *et al.*, 2001, Aubourg and Robion, 2002, Biedermann *et al.*, 2019, Biedermann *et al.*, in review-a, Usui *et al.*, 2006). A recent study illustrates how these coercivity-dependent variations of remanence anisotropy may cause problems for the interpretation of paleodirectional and paleointensity data, and how ApARM based anisotropy corrections can be improved (Biedermann *et al.*, 2019). Similarly, AIRMs can vary with applied field, which may be attributed to anisotropy components carried by different subpopulations of grains. For example, several generations of hematite were found in hematite-bearing Cambrian slates from North Wales, where fine-grained hematite displays stronger fabrics than coarse-grained hematite (Jackson and Borradaile, 1991). Bilardello (2015) used AIRMs determined in different fields to isolate the fabrics of pigmentary and detrital hematite, and also discusses issues related to incomplete saturation of hematite. Alternatively, field-dependent AIRMs in pyrrhotite samples have been explained by competing texture- and grain-size-control of the anisotropy (de Wall and Worm, 1993). Tensor subtraction of the AIRM measured in several fields has been used to calculate the ApIRM of certain coercivity windows (Bogue *et al.*, 1995). Additionally, AIRMs can be partially demagnetized by thermal or AF methods to isolate only the high unblocking temperature or high-coercivity (e.g. hematite) parts of the remanence fabric (Tan and Kodama, 2002, Kodama and

Dekkers, 2004, Bilardello and Kodama, 2009, Bilardello, 2015, Biedermann *et al.*, 2016, Hillhouse, 2010, Cox and Doell, 1967, Tan *et al.*, 2003).

Because magnetization  $M$  saturates in high fields, high-field IRM is not a linear function of the applied field  $H$  or  $B$ . Therefore, it is important to consider how high-field anisotropy is mathematically described. Second-order tensor mathematics, assuming a linear dependence of  $M$  upon  $H$  (Jelinek, 1977), are often used to characterize IRM anisotropy. This is done with the implicit understanding that while this is not strictly correct (Coe, 1966), it remains a useful approximation. Similarly, the low-field susceptibilities of hematite, pyrrhotite and titanomagnetite are field-dependent over the range of AC fields typically used, up to a few hundred A/m ( $H$ ) or  $\mu\text{T}$  ( $B$ ) (de Wall and Worm, 1993, Guerrero-Suarez and Martin-Hernandez, 2012, Jackson *et al.*, 1998, Worm, 1991, de Wall, 2000, Hrouda, 2002a). For these minerals, the magnetic fabric tensors calculated from linear AMS theory may represent an inaccurate description of anisotropy. In some instances, the linear fit to nonlinear data may result in erroneous negative minimum susceptibilities (Hrouda, 2002a). Possible ways to account for the nonlinearity of magnetization with field in these minerals are (1) measuring in extremely low fields,  $< 10$  A/m, where the  $M(H)$  behavior is still linear, (2) measuring many additional orientations and describing the anisotropy using a higher-order tensor, or (3) using the Rayleigh law to compute initial susceptibilities in each orientation, for which tensor calculations are valid (Hrouda, 2002a, Hrouda *et al.*, 2018, Hrouda, 2009). These methods have their own limitations in terms of sensitivity, precision, and efficiency. Whereas the degree of anisotropy can vary strongly with field, principal directions and anisotropy shape, the main parameters used for geologic interpretations, show a weaker field-dependence (Hrouda, 2002a, Hrouda, 2009, de Wall, 2000). Hrouda *et al.* (2018) have compared AMS tensors calculated using linear theory with contour plots from 320 directional susceptibility measurements in various fields for more than 100 specimens, and concluded that the 2<sup>nd</sup>-order tensor describes the specimens' anisotropy to sufficient accuracy. For high-field IRMs and AIRMs, the departure from linearity may be much larger

than for the low-field induced magnetization and low-field AMS, and the effects of treating them with tensor mathematics require further study.

Here, we investigate whether and how the anisotropy of (partial) isothermal remanence (A(p)IRM) varies with coercivity window in different rock types. In addition, we test whether ApIRMs are additive and define error limits for this additivity. The results presented here improve our understanding of isothermal remanence anisotropy, and it is our hope that A(p)IRMs become more useful for studies involving magnetic fabrics and anisotropy corrections.

## 2. Materials and Methods

### 2.1 Sample collection

The sample collection used for this study includes 5 specimens from the Bushveld Complex, South Africa (label prefix BG), 1 specimen from the Bjerkreim Sokndal layered intrusion, Southern Norway (BK), 2 ocean floor gabbros (ODP735), 3 metamorphic slates from the Thomson Formation (TS), and 5 red bed sediment specimens from the Mauch Chunk Formation (MC). The Bushveld samples contain micrometer-sized Ti-magnetite needles and hematite platelets, exsolved within pyroxene and plagioclase. The rocks from Bjerkreim Sokndal contain hemo-ilmenite, either exsolved in pyroxenes or as individual grains, and magnetite. Oceanic gabbros from ODP hole 735B contain both primary Ti-magnetite, and secondary magnetite as exsolutions or formed by alteration of pyroxene and olivine, as well as sulfides. The slates from the Thomson Formation contain magnetite and possibly sulfides, and the red bed sediments contain trace amounts of magnetite, and both detrital and pigmentary hematite. The magnetic mineralogy and anisotropy of susceptibility and anhysteretic remanence of these specimens have been described previously (Feinberg *et al.*, 2006, Biedermann *et al.*, 2016, Pariso and Johnson, 1993, McEnroe *et al.*, 2001, Johns *et al.*, 1992, Sun *et al.*, 1995, Bilardello and Kodama, 2010, Tan and Kodama, 2002, Biedermann *et al.*, in review-a, Biedermann *et al.*, in review-b).

## 2.2 Initial test measurements

For robust anisotropy characterization, it is essential that the directional differences among acquired magnetizations are larger than the variability of repeated measurements along the same direction. Therefore, test measurements were conducted prior to AIRM determination, to check the repeatability of an IRM imparted in a 100 mT field along the specimens' axes. All magnetizations were measured on a 2G 760 superconducting rock magnetometer (SRM). Magnetization tests were performed using a pulse magnetizer (2G, long-core) or a vibrating sample magnetometer (VSM, Princeton Model 3900). For the latter, pick-up coils were removed to obtain a better geometry to fit a sample holder for directional IRMs, maximize the applied field strength, and protect the pick-up coils themselves. Imparting IRMs on a pulse magnetizer is faster, but has the disadvantage that other instruments have to be used to demagnetize the specimens: an AF demagnetizer in low fields, and the electromagnets of a VSM in high fields. The VSM can reach higher fields, but uses a lower frequency than conventional AF units; 10s to 100s of field cycles as compared to 1,000s or 10,000s of field cycles. Concerns have been raised about the accuracy and reproducibility of fields produced by the pulse magnetizer, in particular related to backfield generation at high fields. For example, it has been recommended to use at least 2 pulses to magnetize u-channel samples (Roberts, 2006). Magnetizing specimens on the VSM takes longer, but offers the advantages of better field control, and that specimens can be demagnetized directly on the VSM in fields equal to or slightly above those in which the IRMs were imparted. In this study, repeat measurements of IRMs imparted parallel to x, y, and z were used for the pulse magnetizer, and IRMs along x and y were used for the VSM. For the pulse magnetizer, these test measurements show that (1) the variability of IRMs parallel to any axis is rather large compared to the differences between axes, and (2) the magnetization acquired parallel to the previous axis is not fully remagnetized when the magnetization along the next axis is applied (Figure 1a). This second issue is minimized when demagnetization steps are included between pulse magnetization steps. Similar measurements on the VSM show a smaller variation between repeat measurements (Figure 1b).



Applying progressively higher IRMs up to 1 T along the specimen x-axis reveals an additional difficulty: using the standard mode to turn the field on and off leads to overshooting, i.e., the application of a backfield recoil, resulting in lower IRMs at higher fields. This can be explained by the fact that when applying a higher field, the backfield generated during switch-off of the field is larger. A lower-field pulse, but equal or higher to that of the recoil must be subsequently applied to obviate this effect. The VSM possesses a non-overshoot mode for toggling the field, and this results in IRMs that increase monotonically with applied field and reach saturation, as expected (Figure 1c). Hence, all anisotropy measurements were conducted on the VSM, while toggling the field using the non-overshoot mode.

### 2.3 IRM acquisition

IRM acquisition was characterized on representative samples from each group, selected based on previous A(p)ARM measurements. It was measured following the double IRM acquisition method (Tauxe *et al.*, 1990). This involves applying a field parallel to the specimen +z-axis and measuring the resulting IRM, followed by the same field along the –z-axis, on an initially demagnetized specimen. Based on the results from test measurements, the IRMs were applied on a VSM, and the non-overshoot function was used when turning the fields on and off. Specimens were demagnetized using the VSM's alternating field demagnetization at 1 T (1 % decrement), followed by a second demagnetization at 100 mT (1 % decrement). Acquisition fields were progressively increased from 0 mT, to 5 mT, 10 mT, 20 mT, 35 mT, 50 mT, 75 mT, 100 mT, 130 mT, 180 mT, 240 mT, 320 mT, 410 mT, 500 mT, 630 mT, 800 mT, and 1 T. The last field, 1T along –z, was repeated 3 times to check repeatability. Magnetizations were measured on the 2G-760 SRM, and are reported as x-, y- and z-components, as well as IRM intensity. We will refer to the magnetizations imparted along +z as IRM acquisition, and those along –z as backfield curves.

The coercivity distributions derived from the IRM acquisition curves were analyzed using the MAX Unmix software package (Maxbauer *et al.*, 2016), to separate components of the coercivity

distribution, and determine whether the coercivity spectra contain one or more distinct components. The IRM acquisition curves were not originally collected for coercivity unmixing and contain fewer data points per specimen than is typically recommended. As a result, the precise details of the fitted components should be viewed with a level of caution (e.g., skewness, dispersion, and percent contribution). However, statistical determinations of whether a dataset is best fit by one or more components should remain robust. Unsmoothed spectra were used for all specimens except TS16.2 whose acquired IRM was the weakest, thus subject to a higher noise level.

## 2.4 Anisotropy of full and partial IRMs

A set of 9 (p)IRM anisotropy tensors was determined for each specimen. Each tensor was based on isothermal remanences imparted along 9 directions in a specified field, and partial AF demagnetization of these remanences. The directions used were 0/0 (declination/inclination in specimen coordinates), 90/0, 0/90, 45/0, 135/0, 0/45, 90/45, 180/45, 270/45, following the schemes of McCabe *et al.* (1985) and Girdler (1961) for AARM and AMS, respectively. Directional IRMs were acquired on the VSM in fields of 100 mT, 180 mT, 500 mT, and 1 T. After measuring the full IRM on the 2G-760 SRM, these IRMs were partially demagnetized at 100 mT and 180 mT on a DTech AF demagnetizer and the remaining pIRMs were measured. The fields of 100 mT and 180 mT were chosen because A(p)ARMs have previously been measured in the same fields (Biedermann *et al.*, in review-a, Biedermann *et al.*, in review-b). Note that we are using the term ‘full IRM’ for magnetizations acquired prior to any partial demagnetization, even if a sample’s magnetization does not fully saturate in the fields applied ( $B_{app}$ ). The term ‘partial IRM’ will be used for magnetizations that have been imparted in a field  $B_{app}$  and then AF demagnetized at 100 or 180 mT, i.e. magnetized over the coercivity windows 100 to  $B_{app}$  mT, or 180 to  $B_{app}$  mT. Subsequent to imparting and measuring all IRMs and pIRMs along one direction, the specimens were AF-demagnetized on the VSM at 1 T followed by 100 mT, using 1% decrements, as for the IRM acquisition experiments. The residual magnetization that could not be demagnetized between +1 and -1 T was subtracted from all

directional IRMs as background. AIRM and ApIRM tensors were computed from the parallel components, i.e. the magnetization acquired parallel to the applied field, of each directional magnetization. Thus, each specimen is characterized by 4 AIRMs ( $AIRM_{0-100}$ ,  $AIRM_{0-180}$ ,  $AIRM_{0-500}$ ,  $AIRM_{0-1000}$ ) and 5 ApIRMs ( $ApIRM_{100-180}$ ,  $ApIRM_{100-500}$ ,  $ApIRM_{180-500}$ ,  $ApIRM_{100-1000}$ ,  $ApIRM_{180-1000}$ ). Principal directions, degree and shape of the anisotropy were computed for each A(p)IRM tensor, and compared to one another. The principal directions correspond to the eigenvectors of the magnetization tensor, and the corresponding eigenvalues describe the maximum, intermediate and minimum principal magnetizations ( $M_{max} \geq M_{int} \geq M_{min}$ ). The degree of anisotropy is characterized by two parameters,  $P = \frac{M_{max}}{M_{min}}$  and

$$M' = \sqrt{((M_{max} - M_{mean})^2 + (M_{int} - M_{mean})^2 + (M_{min} - M_{mean})^2)/3}$$

with  $M_{mean} = (M_{max} + M_{int} + M_{min})/3$ , analogously to  $P$  and  $k'$ , respectively, for susceptibility anisotropy. Note that because IRMs saturate in strong fields, we prefer to use magnetizations rather than susceptibilities to define anisotropy parameters. The anisotropy shape is described by  $U = (2 * M_{int} - M_{max} - M_{min}) / (M_{max} - M_{min})$  (Jelinek, 1981, Jelinek, 1984). For the purpose of this study, results are shown in specimen coordinates. Hext (1963)'s statistics was used to determine whether the presence of anisotropy and the directions of principal axes are statistically significant (if  $F < 9.01$  or  $e_{13} > 26^\circ$ , anisotropy is not significant). For subsequent analyses (e.g. tensor addition), statistically insignificant tensors were replaced by an isotropic tensor with diagonal elements equal to  $M_{mean}$ . The orientations of principal axes are at least partially undefined if  $e_{12} > 26^\circ$  or  $e_{23} > 26^\circ$ .

## 2.5 Additivity of ApIRMs

If A(p)IRMs are additive, future studies could determine a small number of individual tensors and then compute additional tensors. To test whether AIRMs are additive, full AIRM tensors for fields  $\geq 180$  mT were computed from sets of measured AIRMs and ApIRMs, and compared to the measured tensors in the same field. Tensors were calculated as follows:

$$AIRM_{0-180,c} = AIRM_{0-100} + ApIRM_{100-180}$$

$$AIRM_{0-500,c1} = AIRM_{0-100} + ApIRM_{100-500}$$

$$AIRM_{0-500,c2} = AIRM_{0-180} + ApIRM_{180-500}$$

$$AIRM_{0-500,c3} = AIRM_{0-100} + ApIRM_{100-180} + ApIRM_{180-500}$$

$$AIRM_{0-1000,c1} = AIRM_{0-100} + ApIRM_{100-1000}$$

$$AIRM_{0-1000,c2} = AIRM_{0-180} + ApIRM_{180-1000}$$

$$AIRM_{0-1000,c3} = AIRM_{0-100} + ApIRM_{100-180} + ApIRM_{180-1000}$$

The group of calculations  $AIRM_{...,c1}$  will be called 0-100-  $B_{app}$ ,  $AIRM_{...,c2}$  are referred to as 0-180-  $B_{app}$ , and  $AIRM_{...,c3}$  as 0-100-180-  $B_{app}$ . Additivity was evaluated in terms of the agreement between mean IRMs, directions of principal axes, anisotropy degree and shape parameter, as well as tensor elements, for the sum of ApIRM and the corresponding measured AIRM tensors. The agreement between summed and directly-measured tensors was quantified by the ratios of calculated and measured values for mean remanence and anisotropy degree, differences for the shape parameter, and angular differences relative to the confidence angles for principal directions, analogously to the assessment of A(p)ARM additivity described in Biedermann *et al.* (in review-b).

### 3. Results

#### 3.1 IRM acquisition and coercivity spectra

Most specimens show a strong initial increase in IRM up to DC fields of 200-300 mT, followed by a weaker increase at higher fields (Figure 2). Specimen MC17\_2, a red bed sediment from the Mauch Chunk formation, does not acquire any IRM in fields < 10 mT, followed by a gradual increase. This specimen does not saturate in a 1 T field, the maximum that could be reached with the pole configuration used on the VSM, and prior work has shown that 4.75 T are necessary to saturate hematite's remanence within and perpendicular to bedding (Bilardello, 2015). In the same specimen,

backfield IRMs are significantly weaker than the IRMs acquired in the same field, which may be due to hematite's multiaxial basal-plane anisotropy (Mitra *et al.*, 2011, Mitra *et al.*, 2012). Similarly, the Thomson Formation slates do not saturate completely in a 1 T field. Unmixing of the coercivity spectra favors two-component models over single components, as indicated by the F-test at 95% confidence (Table A, online supplementary). Additional components at higher fields cannot be excluded. Note that for all specimens, while the IRMs were imparted parallel to the specimens' z-axes, the magnetizations acquired also possess components along the specimen x- and y-axes, which is a direct consequence of remanence anisotropy. Repeat application of an IRM in the same direction leads to a 1.2% to 2.5% increase in magnetization for specimens MC17\_2 and TS16.2 which do not saturate in a 1 T field, and 0.06% to 0.7% change in the remaining specimens. A similar kind of progressive increase in repeated IRM has been observed in treatments of u-channel samples, but attributed to artefacts of the pulse magnetizer (Roberts, 2006). Because we observe changes in IRM acquired on the VSM, and because they are strongest for non-saturated specimens, we argue that small changes occur in magnetization, that seem likely to be time-dependent effects but remain to be fully analyzed.

### 3.2 AIRMs and ApIRMs

Nine tensors each were measured on 16 specimens. The full directional IRMs in one specimen, ODP735.042, were so strong that they could not be measured reliably, so that for this specimen, only the 5 ApIRM tensors are reported. The mean (p)IRMs of specimens that could be measured vary over several orders of magnitude, from  $3.47 \cdot 10^{-7} \text{ Am}^2/\text{kg}$  to  $2.50 \cdot 10^{-2} \text{ Am}^2/\text{kg}$  (Table B, online supplementary). A total of 140 A(p)IRM tensors have been characterized, and 28 of these do not possess statistically significant anisotropy. It is mainly the low-coercivity AIRMs and ApIRMs of the Mauch Chunk red bed samples, and the high-coercivity ApIRMs of the Thomson Slate and ocean floor gabbro that are not significant. A likely explanation for this is that only weak (p)IRMs are acquired by these sample groups in the respective coercivity windows, thus leading to a higher

influence of noise on the anisotropy tensor calculation. The lack of IRM acquisition in low fields or low-field IRM anisotropy in some red bed samples is related to negligible amounts of magnetite, or no magnetite anisotropy, respectively. In contrast, the Thomson Slate and ocean floor gabbro specimens contain predominantly low-coercivity minerals such as magnetite and titanomagnetite, so that the mean high-field pIRMs are weak.

For those specimens that do have significant anisotropy,  $P$  varies between 1.06 and 4.79. The highest  $P$ -values are observed for low-coercivity AIRMs of those Mauch Chunk red bed specimens that seem to display significant anisotropy. It has been shown previously that noise on a weak susceptibility signal can lead to unrealistically high  $P$ -values as well as a large spread in shape parameters for AMS measurements (Biedermann *et al.*, 2013, Hrouda, 2004, Hrouda, 1986). A similar effect may explain the seemingly high  $P$ -values of the  $ARM_{0-100}$ ,  $ARM_{0-180}$ , and  $ApIRM_{100-180}$  in these red beds. The parameter  $M'$  varies between  $7.62 \cdot 10^{-8} \text{ Am}^2/\text{kg}$  and  $1.16 \cdot 10^{-3} \text{ Am}^2/\text{kg}$ , which corresponds to 2.3% to 53% of the mean (p)IRM obtained by the respective specimens in the respective windows. The anisotropy shape  $U$  covers the range from -0.79 to 0.84.

Principal directions, degree and shape of the anisotropy can be similar or vary between different ApIRMs and AIRMs in the same specimen. The principal directions in the Bushveld specimens can have similar orientations, or show two or three distinct sets of directions. In the latter case, the main difference is often between the AIRMs and the ApIRMs, where different coercivity sub-populations may be associated with subsets of exsolved oxide inclusions in silicate minerals like plagioclase and pyroxene. The Bjerkreim Sokndal specimen has similar orientations for all A(p)IRM tensors. The one ODP735 gabbro for which all tensors could be measured, exhibits a switch of maximum and minimum principal directions between AIRM and ApIRM tensors. Two Thomson Slate specimens show similar orientations of all A(p)IRMs, and the third one has different principal directions in the  $ApIRM_{180-Bapp}$  windows as opposed to the AIRM and the  $ApIRM_{100-Bapp}$  where significant. For the Mauch Chunk red beds, 4 specimens display similar orientation for all A(p)IRMs that are significant,

and one specimen shows a similar orientation of the minimum axis, and a girdle distribution of the other two axes (Figure 3).

For most specimens,  $M'$  is highest for the AIRMs followed by the  $ApIRM_{100-B_{app}}$  and  $ApIRM_{180-B_{app}}$ . The one exception to this general trend is the Mauch Chunk red bed sample suite, where the tensors incorporating the highest coercivities, i.e.  $AIRM_{0-1000}$ ,  $ApIRM_{100-1000}$  and  $ApIRM_{180-1000}$ , have the strongest anisotropies. The anisotropy parameters  $M'$ ,  $P$  and  $U$  vary with the field in which the (p)IRM was acquired, and these variations appear consistent between different specimens from the same locality (Figure 4).

### 3.3 Additivity

The calculated mean IRM, obtained by summing the appropriate (p)IRM tensors, is generally lower than the corresponding measured mean IRM. For calculations involving the tensors 0-100- $B_{app}$  and 0-100-180- $B_{app}$  ( $AIRM_{0-180,c}$ ,  $AIRM_{0-500,c1}$ ,  $AIRM_{0-500,c3}$ ,  $AIRM_{0-1000,c1}$ ,  $AIRM_{0-1000,c3}$ ), the ratio of calculated to measured mean IRM can be as low as 0.9. Calculations 0-180- $B_{app}$  ( $AIRM_{0-500,c2}$ ,  $AIRM_{0-1000,c2}$ ) are slightly more accurate, with the calculated mean being  $\geq 0.95$  times the measured mean. The calculated  $M'$  ranges from ca. 0.5 to ca. 1.5 times the measured  $M'$ . Similar to the mean IRM, the variation appears smaller for the 0-180- $B_{app}$  calculations than those based on 0-100- $B_{app}$  and 0-100-180- $B_{app}$ . The variations in shape parameters are about  $\pm 0.5$  (Figure 5). Differences can be observed between the behaviors for each sample group. However, the number of specimens per group was small, so that this observation may be biased by the statistics of small numbers. Hence, they will not be interpreted further.

The angular deviations between the measured and calculated maximum and minimum principal directions are generally smaller than the 95% confidence angles of the measurements for the Mauch Chunk, Thomson slate and ODP735 ocean floor gabbro specimens. The angle between measured and calculated maximum principal directions was compared to the  $e_{12}$  confidence angle, and that between the minimum principal directions to  $e_{23}$  of the measured AIRMs. Because the deviation

between measured and calculated directions is smaller than the confidence angles, the calculated and measured principal directions cannot be statistically distinguished on the 95% confidence level. For most Bushveld specimens and the Bjerkreim Sokndal specimen, however, the angle between calculation and measurement is larger than the confidence angle for at least one of these axes, meaning that the principal directions calculated by tensor addition are significantly different from those measured. In accordance with the other parameters, the difference between measured and calculated principal directions is smallest for the 0-180- $B_{app}$  calculations.

## 4. Discussion

### 4.1 Variation of A(p)IRM with DC field

Similar to the coercivity-dependence of anhysteretic remanence anisotropy (Biedermann *et al.*, in review-a, Biedermann *et al.*, 2019, Jackson *et al.*, 1988, Jackson *et al.*, 1989), isothermal remanence anisotropy varies with the strength of the DC field in which the remanence was acquired. The degree and shape of anisotropy are generally different within each field window. In samples from the Bushveld Complex, the shape parameter  $U$  varies between -0.8 and +0.8, and the degree of anisotropy,  $M'$ , covers the range from 0 to  $1.2 \cdot 10^{-3} \text{ Am}^2/\text{kg}$ , or 0-15% of the mean (p)IRM. Different A(p)IRM subfabrics in the Bjerkreim Sokndal specimen cover shape values between 0.1 and 0.4, and  $M'$  between 0 and  $5.1 \cdot 10^{-4} \text{ Am}^2/\text{kg}$ , up to 12% of the mean (p)IRM. The anisotropy tensors for the ODP735 specimens that could be measured possess  $U$  in the range of -0.6 to +0.3, and  $M'$  in the range of 0 to  $1.1 \cdot 10^{-3} \text{ Am}^2/\text{kg}$ , up to 8% of the mean (p)IRM. Thomson slate specimens display  $U$  from -0.6 to +0.8,  $M'$  from 0 to  $2.1 \cdot 10^{-6} \text{ Am}^2/\text{kg}$ , up to 24% of the mean remanence, and red bed specimens from the Mauch Chunk Formation have  $U$  between -0.2 and +0.8, and  $M'$  between 0 and  $3.6 \cdot 10^{-4} \text{ Am}^2/\text{kg}$  or up to 53% of the mean (p)IRM in the respective windows. Although some uncertainty is associated with each measurement, measurement errors cannot explain the entire variation amongst tensors measured in different fields.



For lithologies where more than 3 specimens were measured, there are smaller variations between anisotropy parameters measured in each field window on all specimens from the site compared to those seen in the same specimen but for different windows (Figure 6). Therefore, differences between anisotropy parameters measured in specific field windows can be interpreted as discrete subpopulations of grains – defined by their mineralogy, composition, grain size and shape – having distinct fabrics. Bilardello (2015) had investigated changes of anisotropy degree and shape with coercivity during a stepwise demagnetization of IRMs acquired in 1 and 5.5 T fields on Mauch Chunk samples from the same location as those studied here. That study attributed changes in anisotropy parameters to (1) non-saturation of hematite in 1 T fields, and (2) differences in coercivity of specular versus pigmentary hematite and additional accessory magnetite. The present study shows further examples of rocks whose IRM anisotropy varies with DC field, also when magnetite or iron sulfides dominate the anisotropy. Whether these results are directly relevant to other magnetic fabric investigations, depends on the main focus of those studies, the mineral populations present, and the fields needed to saturate their remanence. In any case, the results presented here lay a solid foundation for future work on the field dependence of IRM anisotropy.

Analogous to AMS and A(p)ARM, the highest anisotropy is not necessarily carried by the same grain fraction as the highest mean (p)IRM. The same specimen can display significant anisotropy in some coercivity windows, but not in others, and the A<sub>p</sub>IRMs carried by different sub-populations can add up or cancel each other out. Therefore, care needs to be taken when interpreting AIRMs in fabric studies, because similar to AMS or AARM, they can reflect composite fabrics. For the same reason, the field in which A(p)IRMs are measured needs to be chosen carefully when these tensors are used in paleomagnetic and paleointensity studies to correct for anisotropic remanence acquisition in high-coercivity grains. Isolating an appropriate anisotropy tensor prior to anisotropy corrections is crucial, as these corrections can have major implications for apparent polar wander paths (Bilardello and Kodama, 2010). When the remanence is carried by a combination of sub-populations, paleomagnetic results are further affected by differences in remanence anisotropy between carriers, which needs

to be taken into account during anisotropy corrections (Biedermann *et al.*, 2019). Breaking down the full AIRM to individual ApIRMs can help determine how remanence anisotropy changes for each subpopulation in the specimen, and provides a solid basis for the reliable interpretation of both fabric and paleomagnetic data. A solid indication that a specimen possesses a composite IRM anisotropy is when the magnetization direction changes during an IRM acquisition or IRM demagnetization experiment. Note that the absence of changes in magnetization direction is not a reliable indicator for the absence of multiple contributors to AIRM, as the fabrics could be aligned but have different anisotropy degrees.

## 4.2 ApIRM additivity

Mean IRMs are underestimated when calculated from tensor addition of ApIRMs, especially when the added tensors contain the terms  $AIRM_{0-100} + ApIRM_{100-Bapp}$ . In this study, errors can be as high as 10% of the measured mean IRM. Smaller errors,  $\leq 5\%$ , are observed when adding  $AIRM_{0-180} + ApIRM_{180-Bapp}$ . The latter error limit is of similar magnitude to that for mean ARM additivity (Yu *et al.*, 2002, Biedermann *et al.*, in review-b). One possible reason for the variation of error with field is that the IRM varies strongly with field before specimens reach saturation at around 200-300 mT, but little variation of IRM with DC field is observed for higher fields, when the low-coercivity grains are saturated. Therefore, a small variability in DC field when imparting the IRM, will have a larger effect on the acquired remanence at 100 mT than at higher fields. Analogously, if the AF demagnetizing field slightly deviates from the set field during a partial AF demagnetization, the effect will be larger at 100 mT than 180 mT. Because the calculated AIRMs are lower than those measured, the initially applied field may have been slightly too low, or the demagnetizing field too high, both attributable to instrumental precision. This hypothesis can be further investigated and resolved once instrumentation has been developed that produces reliable and repeatable IRM fields. More reliable and reproducible IRM fields would also be beneficial for double-IRM acquisition experiments (Tauxe *et al.*, 1990), and would prevent researchers from having to use several pulses to impart IRMs

(Roberts, 2006). A second possibility is that slight misalignment of the samples when imparting directional pIRMs would lead to a smaller added directional IRM, and eventually a weaker added mean IRM compared to that measured. Although samples were carefully oriented in a specially designed holder for these measurements, small errors cannot be excluded completely. Another possible explanation for better additivity in the 0-180- $B_{app}$  calculations compared to 0-100- $B_{app}$  and 0-100-180- $B_{app}$ , is that the pIRMs may not be fully independent: if this is the case, the effect on magnetization is larger at low fields where grains are not saturated than at high fields where they approach saturation or have saturated already. Further work needs to be conducted to investigate whether pIRMs are independent.

The main difference between AARM and AIRM measurements is that ARMs are usually weak enough to behave linearly with the field, whereas strong-field isothermal remanences begin to approach saturation and thus are not linear with the applied field. Fitting a linear tensor equation to this nonlinear data may introduce errors, similar to and larger than those described for low-field AMS in field-dependent materials (Hrouda, 2002a). It is possible that the larger uncertainty in AIRM additivity stems from the nonlinearity of the directional IRMs with applied field. This would result in a correlation between tensor misfit (of either the ApIRM tensors used in the calculation, or the AIRM tensor the calculation is compared to) and the deviation of the calculated tensor from the measured tensor. The grouping of our data makes it hard to draw a general conclusion whether the uncertainty is related to tensor misfit. However, there appear to be larger deviations between calculated and measured mean IRMs when the tensor misfit is larger, and there is also more scatter for larger tensor misfits (Figure 7). Similarly, larger scatter and larger deviations may be observed for other anisotropy parameters with increasing tensor misfit, but more data would be needed to make a general statement about the exact nature of such a correlation.

The error limits for principal directions and anisotropy parameters for A(p)IRM additivity are generally larger than the corresponding error limits determined for A(p)ARM on the same specimens

(Biedermann *et al.*, in review-b). Nevertheless, similar to A(p)ARM additivity, principal directions match best between measurement and calculation, followed by degree of anisotropy and anisotropy shape. Therefore, when A(p)IRMs are to be used for anisotropy corrections, where all anisotropy parameters influence the final results and are thus important, we suggest that all necessary AIRMs and ApIRMs be measured directly, by imparting a set of directional IRMs followed by partial AF or thermal demagnetization, rather than derived from tensor addition and subtraction. In fabric studies with a main focus on the orientation of principal directions, rather than the exact values of  $P$ ,  $M'$  and  $U$ , tensor calculations may be sufficient for a structural interpretation.

## 5. Conclusions

A total of 140 A(p)IRM tensors have been measured on 16 specimens from five geological settings. The samples were chosen to cover a range of remanence carriers and coercivity spectra. The results shown here illustrate that principal directions, degree and shape of AIRM and ApIRM depend on the coercivity window over which the remanence was imparted. This indicates that various subpopulations of grains together carry the remanence, and each of them possesses a distinct magnetic fabric. Hence, characterizing ApIRMs in addition to full AIRMs allows for more detailed tectonic and structural interpretations, and forms the basis for more advanced and accurate corrections of paleomagnetic data.

Tensor additions of A(p)IRMs generally underestimate the mean IRM compared to a direct AIRM measurement. The level of underestimation depends on whether individual ApIRM windows were chosen at low fields, before the specimen starts to approach saturation, or higher fields close to or above saturation. Error limits are larger in the former case. This may be related to small variability in the field generated to impart IRMs, which underscores the importance of developing more advanced instrumentation that can produce exact and repeatable fields. Another possibility that needs further work, is that pIRMs may not be fully independent. A third explanation, which will also need to be investigated further, is that the differences between measured and calculated parameters are

related to the nonlinearity of isothermal magnetization with field. This nonlinearity means that second-order tensors are strictly not correct representations of the anisotropy, which results in misfits when calculating the tensor from the directional data.

For most specimens, calculated principal directions for summed pIRM tensors are within the 95% confidence ellipses for the measured total AIRM. Error limits for anisotropy degree and shape can be as large as  $\pm 50\%$  and  $\pm 0.5$ , respectively. Therefore, calculated AIRMs or ApIRMs may be suitable for fabric interpretations; however, we recommend measuring each tensor directly for paleomagnetic corrections.

## Acknowledgements

Fatima Martin-Hernandez and Pedro Silva are thanked for their thoughtful and constructive reviews. This research was funded by the Swiss National Science Foundation, project 167608, and measurements were conducted at the IRM. The IRM is a US National Multi-user Facility supported through the Instrumentation and Facilities program of the National Science Foundation, Earth Sciences Division, and by funding from the University of Minnesota. Data is available from the online supplementary. This is IRM publication 1811.

## References

- Agro, A., Zanella, E., Le Pennec, J.-L. & Temel, A., 2017. Complex remanent magnetization in the Kizilkaya ignimbrite (central Anatolia): Implication for paleomagnetic directions, *Journal of Volcanology and Geothermal Research*, 336, 68-80.
- Aubourg, C. & Robion, P., 2002. Composite ferromagnetic fabrics (magnetite, greigite) measured by AMS and partial AARM in weakly strained sandstones from western Makran, Iran, *Geophysical Journal International*, 151, 729-737.
- Bascou, J., Raposo, M.I.B., Vauchez, A. & Egydio-Silva, M., 2002. Titanohematite lattice-preferred orientation and magnetic anisotropy in high-temperature mylonites, *Earth and Planetary Science Letters*, 198, 77-92.
- Biedermann, A.R., Bilardello, D., Jackson, M., Tauxe, L. & Feinberg, J.M., 2019. Grain-size-dependent remanence anisotropy and its implications for paleodirections and paleointensities - proposing a new approach to anisotropy corrections, *Earth and Planetary Science Letters*, 512, 111-123.

- Biedermann, A.R., Heidelbach, F., Jackson, M., Bilardello, D. & McEnroe, S.A., 2016. Magnetic fabrics in the Bjerkreim Sokndal Layered Intrusion, Rogaland, southern Norway: Mineral sources and geological significance, *Tectonophysics*, 688, 101-118.
- Biedermann, A.R., Jackson, M., Bilardello, D. & Feinberg, J.M., in review-a. Anisotropy of full and partial anhysteretic remanence across different rock types: 2. Coercivity-dependence of remanence anisotropy, *Tectonics*.
- Biedermann, A.R., Jackson, M., Stillinger, M.D., Bilardello, D. & Feinberg, J.M., in review-b. Anisotropy of full and partial anhysteretic remanence across different rock types: 1. Are partial anhysteretic remanence anisotropy tensors additive?, *Tectonics*.
- Biedermann, A.R., Lowrie, W. & Hirt, A.M., 2013. A method for improving the measurement of low-field magnetic susceptibility anisotropy in weak samples, *Journal of Applied Geophysics*, 88, 122-130.
- Bilardello, D., 2015. Isolating the anisotropy of the characteristic remanence-carrying hematite grains: a first multispecimen approach, *Geophysical Journal International*, 202, 695-712.
- Bilardello, D. & Jackson, M.J., 2014. A comparative study of magnetic anisotropy measurement techniques in relation to rock-magnetic properties, *Tectonophysics*, 629, 39-54.
- Bilardello, D. & Kodama, K.P., 2009. Measuring remanence anisotropy of hematite in red beds: anisotropy of high-field isothermal remanence magnetization (hf-AIR), *Geophysical Journal International*, 178, 1260-1272.
- Bilardello, D. & Kodama, K.P., 2010. A new inclination shallowing correction of the Mauch Chunk Formation of Pennsylvania, based on high-field AIR results: Implications for the Carboniferous North American APW path and Pangea reconstructions, *Earth and Planetary Science Letters*, 299, 218-227.
- Bogue, S.W., Gromme, S. & Hillhouse, J.W., 1995. Paleomagnetism, magnetic anisotropy, and mid-Cretaceous paleolatitude of the Duke Island (Alaska) ultramafic complex, *Tectonics*, 14, 1133-1152.
- Borradaile, G.J. & Dehls, J.F., 1993. Regional kinematic inferred from magnetic subfabrics in Archean rocks of Northern Ontario, Canada, *Journal of Structural Geology*, 15, 887-894.
- Borradaile, G.J. & Henry, B., 1997. Tectonic applications of magnetic susceptibility and its anisotropy, *Earth-Science Reviews*, 42, 49-93.
- Borradaile, G.J. & Jackson, M., 2010. Structural geology, petrofabrics and magnetic fabrics (AMS, AARM, AIRM), *Journal of Structural Geology*, 32, 1519-1551.
- Cagnoli, B. & Tarling, D., 1997. The reliability of anisotropy of magnetic susceptibility (AMS) data as flow direction indicators in friable base surge and ignimbrite deposits: Italian examples, *Journal of Volcanology and Geothermal Research*, 75, 309-320.
- Coe, R.S., 1966. Analysis of magnetic shape anisotropy using second-rank tensors, *Journal of Geophysical Research*, 71, 2637-2644.
- Cox, A. & Doell, R.R., 1967. Measurement of high-coercivity magnetic anisotropy. in *Methods in Palaeomagnetism*, pp. 477-482, eds. Collinson, D. W., Creer, K. M. & Runcorn, S. K. Elsevier Publishing Company, Amsterdam, NL.
- Cramer, F., 2018. Geodynamic diagnostics, scientific visualisation and StagLab 3.0, *Geoscientific Model Development*, 11, 2541-2562.
- de Wall, H., 2000. The field dependence of AC susceptibility in titanomagnetites: implications for the anisotropy of magnetic susceptibility, *Geophysical Research Letters*, 27, 2409-2411.
- de Wall, H. & Worm, H.-U., 1993. Field dependence of magnetic anisotropy in pyrrhotite: effects of texture and grain shape, *Physics of the Earth and Planetary Interiors*, 76, 137-149.
- di Capua, A., 2014. Volcanism versus tectonics in the sedimentary record, PhD, Università degli studi di Milano-Bicocca, Milan, Italy.
- Feinberg, J.M., Wenk, H.-R., Scott, G.R. & Renne, P.R., 2006. Preferred orientation and anisotropy of seismic and magnetic properties in gabbro-norites from the Bushveld layered intrusion, *Tectonophysics*, 420, 345-356.

- Font, E., Trindade, R.I.F. & Nédélec, A., 2005. Detrital remanent magnetization in haematite-bearing Neoproterozoic Puga cap dolostone, Amazon craton: a rock magnetic and SEM study, *Geophysica Journal International*, 163, 491-500.
- Garrick-Bethell, I., Weiss, B.P., Shuster, D.L., Tikoo, S.M. & Tremblay, M.M., 2016. Further evidence for early lunar magnetism from troctolite 76535, *Journal of Geophysical Research: Planets*, 121.
- Girdler, R.W., 1961. The measurement and computation of anisotropy of magnetic susceptibility in rocks, *Geophysical Journal of the Royal Astronomical Society*, 5, 34-44.
- Guerrero-Suarez, S. & Martin-Hernandez, F., 2012. Magnetic anisotropy of hematite natural crystals: increasing low-field strength experiments, *International Journal of Earth Sciences*, 101, 625-636.
- Henry, B. & Daly, L., 1983. From qualitative to quantitative magnetic anisotropy analysis: The prospect of finite strain calibration, *Tectonophysics*, 98, 327-336.
- Hext, G.R., 1963. The estimation of second-order tensors, with related tests and designs, *Biometrika*, 50, 353-373.
- Hillhouse, J.W., 2010. Clockwise rotation and implications for northward drift of the western Transverse Ranges from paleomagnetism of the Piuma Member, Sespe Formation, near Malibu, California, *Geochemistry Geophysics Geosystems*, 11, Q07005.
- Hodych, J.P. & Buchan, K.L., 1994. Early Silurian palaeolatitude of the Springdale Group redbeds of central Newfoundland: a palaeomagnetic determination with a remanence anisotropy test for inclination error, *Geophysical Journal International*, 117, 640-652.
- Hrouda, F., 1982. Magnetic anisotropy of rocks and its application in geology and geophysics, *Geophysical Surveys*, 5, 37-82.
- Hrouda, F., 1986. The effect of quartz on the magnetic anisotropy of quartzite, *Studia Geophysica Et Geodaetica*, 30, 39-45.
- Hrouda, F., 2002a. Low-field variation of magnetic susceptibility and its effect on the anisotropy of magnetic susceptibility of rocks, *Geophysica Journal International*, 150, 715-723.
- Hrouda, F., 2002b. The use of the anisotropy of magnetic remanence in the resolution of the anisotropy of magnetic susceptibility into its ferromagnetic and paramagnetic components, *Tectonophysics*, 347, 269-281.
- Hrouda, F., 2004. Problems in interpreting AMS parameters in diamagnetic rocks. in *Magnetic Fabric: Methods and Applications*, pp. 49-59, eds. Martín-Hernández, F., Lüneburg, C. M., Aubourg, C. & Jackson, M. The Geological Society, London, UK.
- Hrouda, F., 2009. Determination of field-independent and field-dependent components of anisotropy of susceptibility through standard AMS measurement in variable low fields I: Theory, *Tectonophysics*, 466, 114-122.
- Hrouda, F., Chadima, M. & Jezek, J., 2018. Anisotropy of susceptibility in rocks which are magnetically nonlinear even in low fields, *Geophysica Journal International*, 213, 1792-1803.
- Hrouda, F., Henry, B. & Borradaile, G.J., 2000. Limitations of tensor subtraction in isolating diamagnetic fabrics by magnetic anisotropy, *Tectonophysics*, 322, 303-310.
- Jackson, M. & Borradaile, G., 1991. On the origin of the magnetic fabric in purple Cambrian slates of North Wales, *Tectonophysics*, 194, 49-58.
- Jackson, M., Gruber, W., Marvin, J. & Banerjee, S.K., 1988. Partial anhysteretic remanence and its anisotropy: applications and grain-size-dependence, *Geophysical Research Letters*, 15, 440-443.
- Jackson, M., Moskowitz, B., Rosenbaum, J. & Kissel, C., 1998. Field-dependence of AC susceptibility in titanomagnetites, *Earth and Planetary Science Letters*, 157, 129-139.
- Jackson, M., Sprowl, D. & Ellwood, B., 1989. Anisotropies of partial anhysteretic remanence and susceptibility in compacted black shales: grain-size- and composition-dependent magnetic fabric, *Geophysical Research Letters*, 16, 1063-1066.

- Jackson, M. & Tauxe, L., 1991. Anisotropy of magnetic susceptibility and remanence: Developments in the characterization of tectonic, sedimentary, and igneous fabric, *Reviews of Geophysics*, 29, 371-376.
- Jackson, M.J., 1991. Anisotropy of magnetic remanence: A brief review of mineralogical sources, physical origins, and geological applications, and comparison with susceptibility anisotropy, *Pure and Applied Geophysics*, 136, 1-28.
- Jelinek, V., 1977. The statistical theory of measuring anisotropy of magnetic susceptibility of rocks and its application.
- Jelinek, V., 1981. Characterization of the magnetic fabric of rocks, *Tectonophysics*, 79, T63-T67.
- Jelinek, V., 1984. On a mixed quadratic invariant of the magnetic susceptibility tensor, *Journal of Geophysics - Zeitschrift Fur Geophysik*, 56, 58-60.
- Johns, M.K., Jackson, M.J. & Hudleston, P.J., 1992. Compositional control of magnetic anisotropy in the Thomson formation, east-central Minnesota, *Tectonophysics*, 210, 45-58.
- Kodama, K.P. & Dekkers, M.J., 2004. Magnetic anisotropy as an aid to identifying CRM and DRM in red sedimentary rocks, *Studia Geophysica Et Geodaetica*, 48, 747-766.
- Kovacheva, M., Chauvin, A., Jordanova, N., Lanos, P. & Karloukovski, V., 2009. Remanence anisotropy effect on the palaeointensity results obtained from various archaeological materials, excluding pottery, *Earth Planets Space*, 61, 711-732.
- Lawrence, R.M., Gee, J.S. & Karson, J.A., 2002. Magnetic anisotropy of serpentinized peridotites from the MARK area: Implications for the orientation of mesoscopic structures and major fault zones, *Journal of Geophysical Research*, 107, 2073.
- Lu, G. & McCabe, C., 1993. Magnetic fabric determined from ARM and IRM anisotropies in Paleozoic carbonates, Southern Appalachian Basin, *Geophysical Research Letters*, 20, 1099-1102.
- Lycka, R., 2017. A Systematic Comparison of the Anisotropy of Magnetic Susceptibility (AMS) and Anisotropy of Remanence (ARM) Fabrics of Ignimbrites: Examples from the Quaternary Bandelier Tuff, Jemez Mountains, New Mexico and Miocene Ignimbrites near Gold Point, Nevada, MS thesis, UT Dallas.
- Martín-Hernández, F. & Ferré, E.C., 2007. Separation of paramagnetic and ferrimagnetic anisotropies: A review, *Journal of Geophysical Research-Solid Earth*, 112.
- Martín-Hernández, F., Lüneburg, C.M., Aubourg, C. & Jackson, M., 2004. *Magnetic Fabrics: Methods and Applications*, edn, Vol. 238, pp. Pages, The Geological Society, London, UK.
- Maxbauer, D.P., Feinberg, J.M. & Fox, D.L, 2016. MAX UnMix: A web application for unmixing magnetic coercivity distributions, *Computers & Geosciences*, 95, 140-145.
- McCabe, C., Jackson M.J. & Ellwood, B.B., 1985. Magnetic anisotropy in the Trenton limestone: results of a new technique, anisotropy of anhysteretic susceptibility, *Geophysical Research Letters*, 12, 333-336.
- McCall, A.M. & Kodama, K.P., 2014. Anisotropy-based inclination correction for the Moenave Formation and Wingate Sandstone: implications for Colorado Plateau rotation, *Frontiers in Earth Science*, 2.
- McEnroe, S.A., Robinson, P. & Panish, P.T., 2001. Aeromagnetic anomalies, magnetic petrology, and rock magnetism of hemo-ilmenite- and magnetite-rich cumulate rocks from the Sokndal Region, South Rogaland, Norway, *American Mineralogist*, 86, 1447-1468.
- Mitra, R., Tauxe, L. & Gee, J.S., 2011. Detecting uniaxial single domain grains with a modified IRM technique, *Geophysica Journal International*, 187, 1250-1258.
- Mitra, R., Tauxe, L. & Gee, J.S., 2012. Reply to the comment by K. Fabian on 'Detecting uniaxial single domain grains with a modified IRM technique', *Geophysica Journal International*, 191, 46-50.
- Owens, W.H., 1974. Mathematical model studies on factors affecting the magnetic anisotropy of deformed rocks, *Tectonophysics*, 24, 115-131.
- Pariso, J.E. & Johnson, H.P., 1993. Do lower crustal rocks record reversals of the Earth's magnetic field? Magnetic Petrology of Oceanic Gabbros from Ocean Drilling Program Hole 735B, *Journal of Geophysical Research*, 98, 16013-16032.



- Potter, D.K., 2004. A comparison of anisotropy of magnetic remanence methods - a user's guide for application to paleomagnetism and magnetic fabric studies. in *Magnetic Fabrics: Methods and Applications*, pp. 21-35, eds. Martín-Hernández, F., Lüneburg, C. M., Aubourg, C. & Jackson, M. The Geological Society, London, UK.
- Raposo, M.I.B., Chaves, A.O., Lojkasek-Lima, P., D'Agrella-Filho, M.S. & Teixeira, W., 2004. Magnetic fabrics and rock magnetism of Proterozoic dike swarm from the southern Sao Francisco Craton, Minas Gerais State, Brazil, *Tectonophysics*, 378, 43-63.
- Raposo, M.I.B., D'Agrella-Filho, M.S. & Siqueira, R., 2003. The effect of magnetic anisotropy on paleomagnetic directions in high-grade metamorphic rocks from the Juiz de Fora Complex, SE Brazil, *Earth and Planetary Science Letters*, 209, 131-147.
- Roberts, A.P., 2006. High-resolution magnetic analysis of sediment cores: Strengths, limitations and strategies for maximizing the value of long-core magnetic data, *Physics of the Earth and Planetary Interiors*, 156, 162-178.
- Rochette, P., Jackson, M. & Aubourg, C., 1992. Rock magnetism and the interpretation of anisotropy of magnetic susceptibility, *Reviews of Geophysics*, 30, 209-226.
- Selkin, P.A., Gee, J.S., Tauxe, L., Meurer, W.P. & Newell, A.J., 2000. The effect of remanence anisotropy on paleointensity estimates: a case study from the Archean Stillwater Complex, *Earth and Planetary Science Letters*, 183, 403-416.
- Stephenson, A., Sadikun, S. & Potter, D.K., 1986. A theoretical and experimental comparison of the anisotropies of magnetic susceptibility and remanence in rocks and minerals, *Geophysical Journal of the Royal Astronomical Society*, 84, 185-200.
- Stokking, L.B. & Tauxe, L., 1990. Properties of chemical remanence in synthetic hematite: Testing theoretical predictions, *Journal of Geophysical Research*, 95, 12639-12652.
- Sun, W., Hudleston, P.J. & Jackson, M., 1995. Magnetic and petrographic studies in the multiply deformed Thomson Formation, east-central Minnesota, *Tectonophysics*, 249, 109-124.
- Tamaki, M. & Itoh, Y., 2008. Tectonic implications of paleomagnetic data from upper Cretaceous sediments in the Oyubari area, central Hokkaido, Japan, *Island Arc*, 17, 270-284.
- Tan, X. & Kodama, K., 2002. Magnetic anisotropy and paleomagnetic inclination shallowing in red beds: evidence from the Mississippian Mauch Chunk Formation, Pennsylvania, *Journal of Geophysical Research - Solid Earth*, 107, EPM9-1 - EPM9-17.
- Tan, X., Kodama, K.P., Chen, H., Fang, D., Sun, D. & Li, Y., 2003. Paleomagnetism and magnetic anisotropy of Cretaceous red beds from the Tarim Basin, northwest China: Evidence for a rock magnetic cause of anomalously shallow paleomagnetic inclinations from central Asia, *Journal of Geophysical Research - Solid Earth*, 108, 2107.
- Tarling, D.H. & Hrouda, F., 1993. *The magnetic anisotropy of rocks*, edn, Vol., pp. Pages, Chapman and Hall, London, UK.
- Tauxe, L., Constable, C., Stokking, L. & Badgley, C., 1990. Use of anisotropy to determine the origin of characteristic remanence in the Siwalik Red Beds of Northern Pakistan, *Journal of Geophysical Research*, 95, 4391-4404.
- Tema, E., 2009. Estimate of the magnetic anisotropy effect on the archaeomagnetic inclination of ancient bricks, *Physics of the Earth and Planetary Interiors*, 176, 213-223.
- Tikoo, S.M., Weiss, B.P., Buz, J., Lima, E.A., Shea, E.K., Melo, G. & Grove, T.L., 2012. Magnetic fidelity of lunar samples and implications for an ancient core dynamo, *Earth and Planetary Science Letters*, 337-338, 93-103.
- Trindade, R.I.F., Bouchez, J.-L., Bolle, O., Nédélec, A., Peschler, A. & Poitrasson, F., 2001. Secondary fabrics revealed by remanence anisotropy: methodological study and examples from plutonic rocks, *Geophysica Journal International*, 147, 310-318.
- Usui, Y., Nakamura, N. & Yoshida, T., 2006. Magnetite microexsolutions in silicate and magmatic flow fabric of the Goyozan granitoid (NE Japan): Significance of partial remanence anisotropy, *Journal of Geophysical Research*, 111, B11101.

Worm, H.-U., 1991. Multidomain susceptibility and anomalously strong low field dependence of induced magnetization in pyrrhotite, *Physics of the Earth and Planetary Interiors*, 69, 112-118.

Yu, Y., Dunlop, D.J. & Özdemir, Ö., 2002. Partial anhysteretic remanent magnetization in magnetite - 1. Additivity, *Journal of Geophysical Research*, 107, 2244.

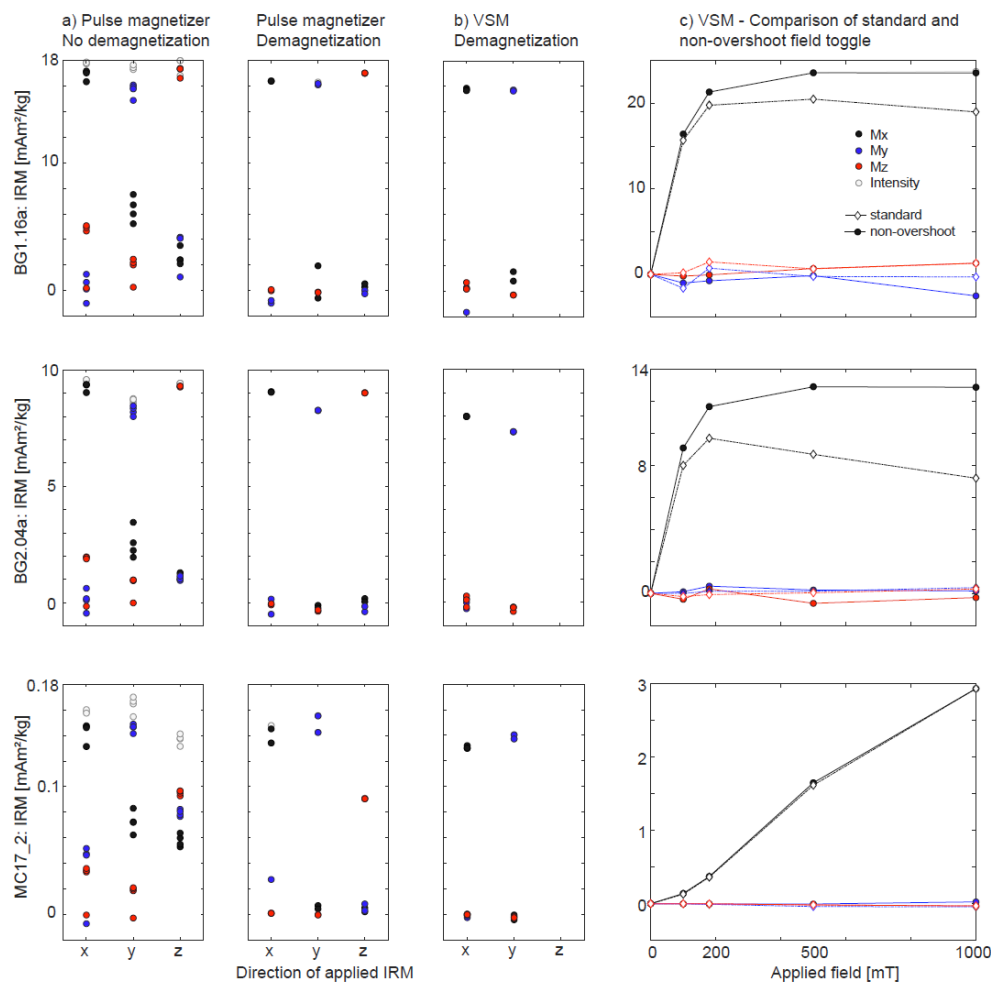


Figure 1: (a) Repeat IRM measurements parallel to the x, y, and z-axes using a pulse magnetizer, with and without AF demagnetization in-between steps. (b) Repeat IRM measurements parallel to x and y on the VSM. (c) Comparison of standard and non-overshoot modes of the VSM for IRMs applied parallel to x.

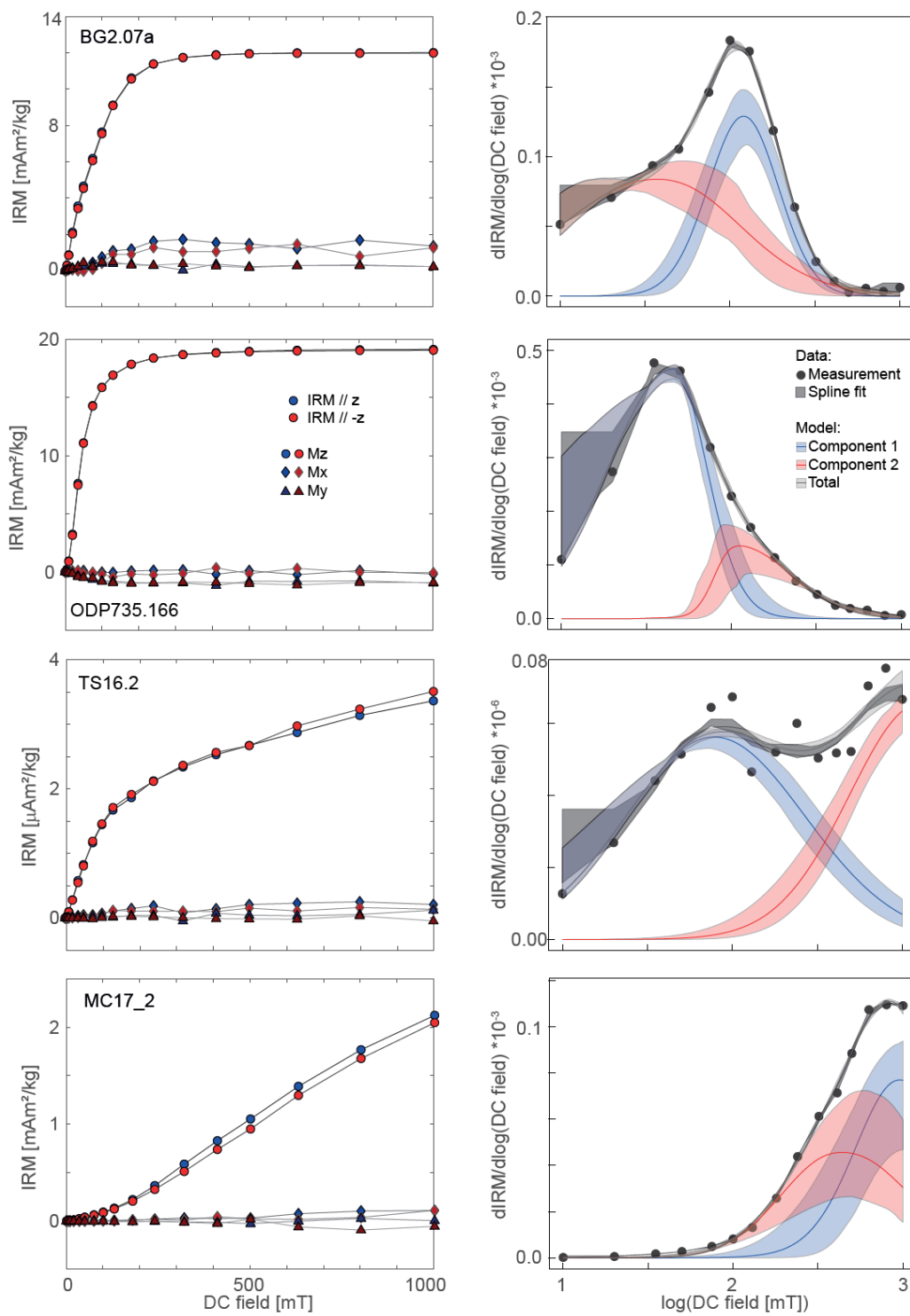
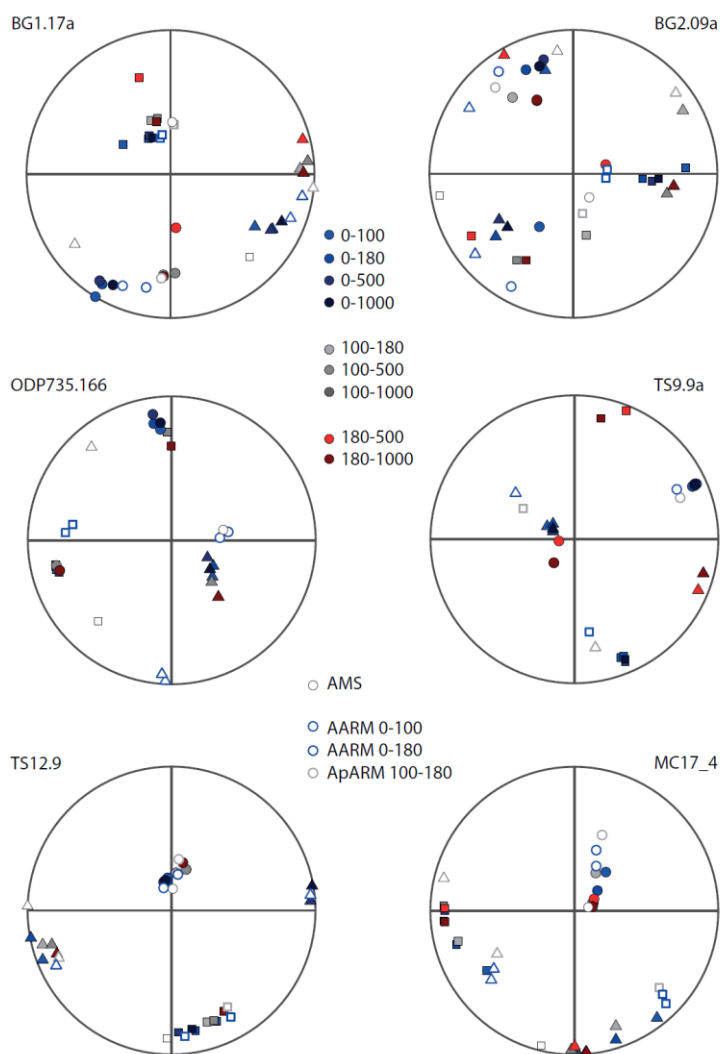


Figure 2: (left column) IRM acquisition and backfield curves for selected specimens. The magnetization was applied parallel to +z (acquisition) and -z (backfield); (right column) Coercivity distribution and unmixing of magnetic components. The contribution of each component as well as their total coercivity spectra are shown as median distributions with 95% confidence limits.



*Figure 3: Principal directions of the AIRM and ApIRM tensors for a selection of representative specimens. Squares, triangles, and circles represent the maximum, intermediate and minimum magnetization directions, and colors refer to the windows over which the (p)IRMs were imposed. Open symbols are the corresponding AARM, ApARM and AMS fabrics reported by Biedermann et al. (in review-a).*

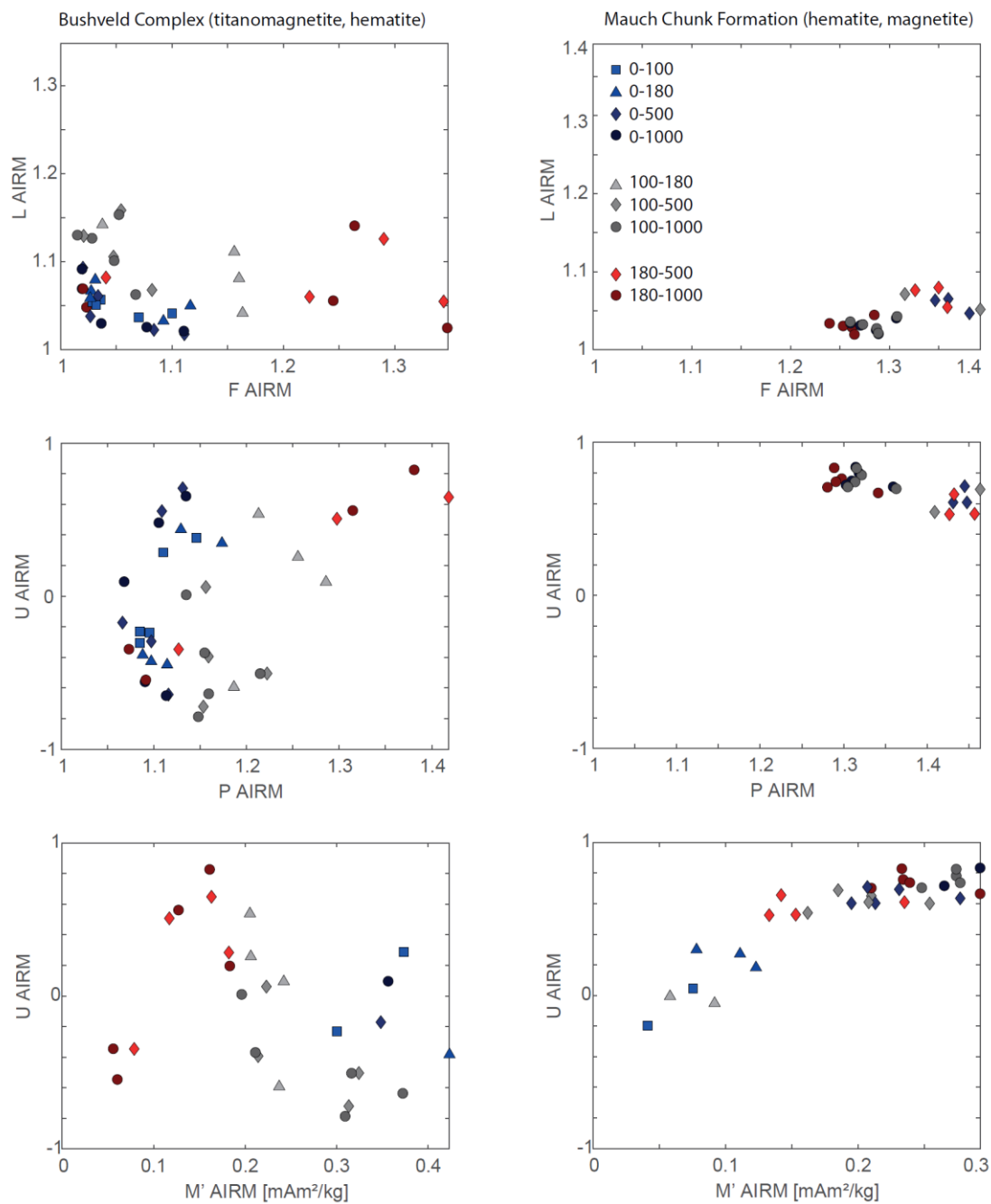


Figure 4: Anisotropy parameters of  $A(p)$ IRMs as a function of coercivity window for representative sample groups.

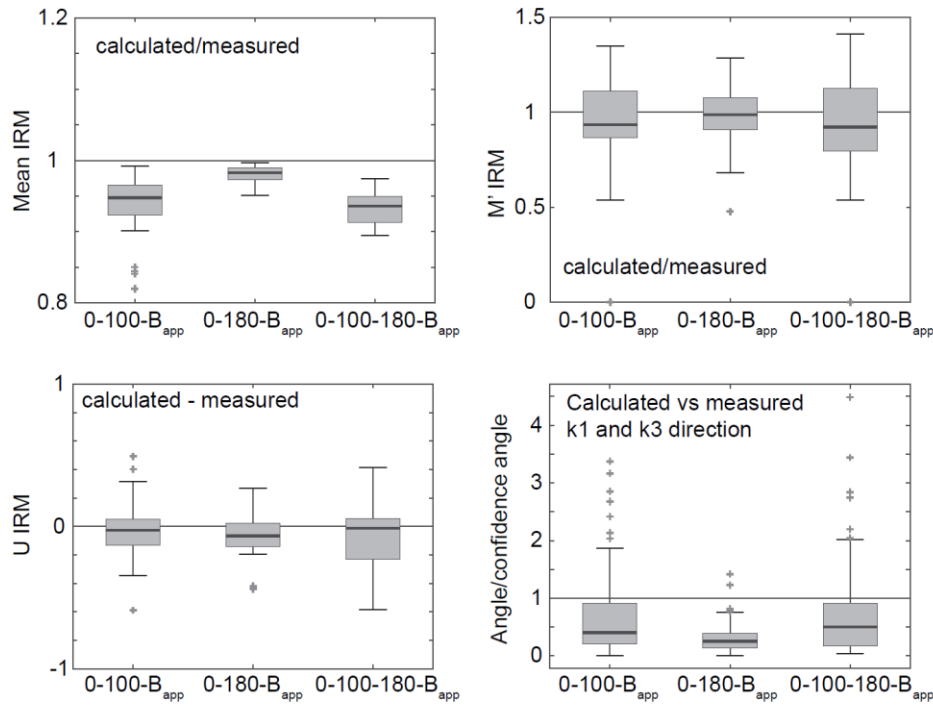


Figure 5: Comparison of calculated anisotropy parameters to measured anisotropy parameters. Black line indicates median, box contains the data from the 25<sup>th</sup> to 75<sup>th</sup> percentile, and whiskers extend to the last data point within 1.5 times the interquartile range. The latter corresponds to 99% of the data points as long as data are normally distributed. Crosses show data points considered as outliers.

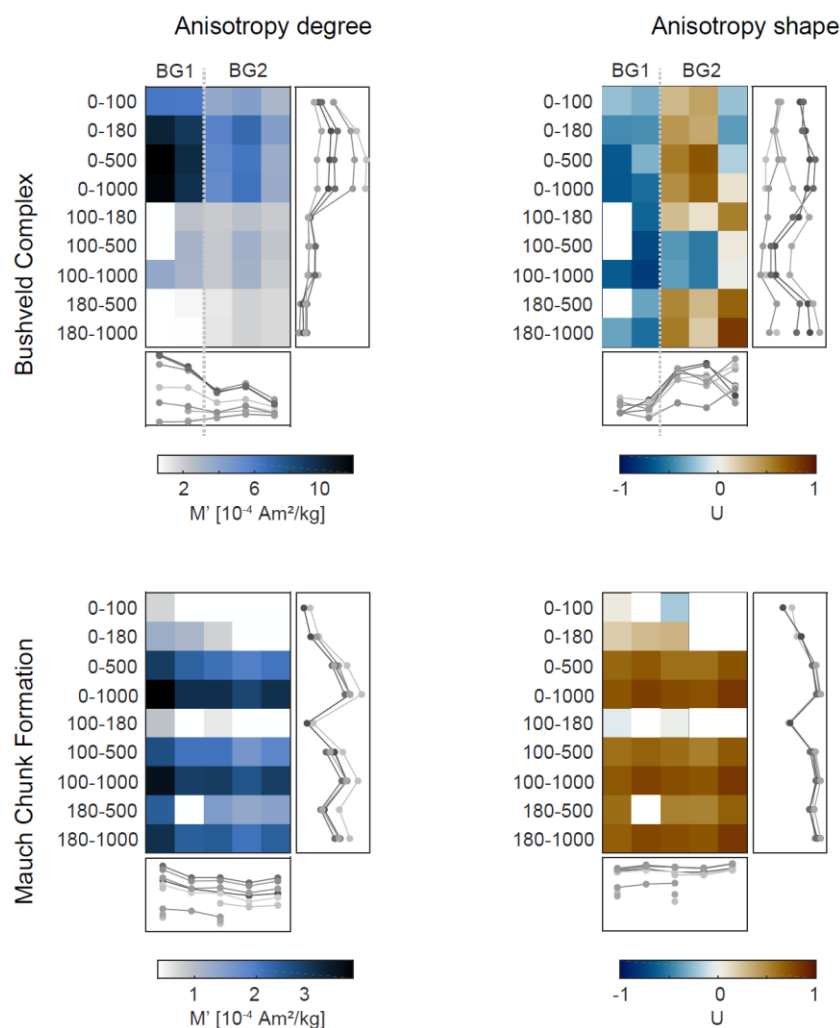


Figure 6: Anisotropy degree and shape of the Bushveld and Mauch Chunk samples. Variations with DC field compared to variations between different specimens and sites. White indicates fields and specimens whose anisotropy was not statistically significant. Perceptually uniform color-maps are used to prevent visual distortion of the data (Crameri, 2018).



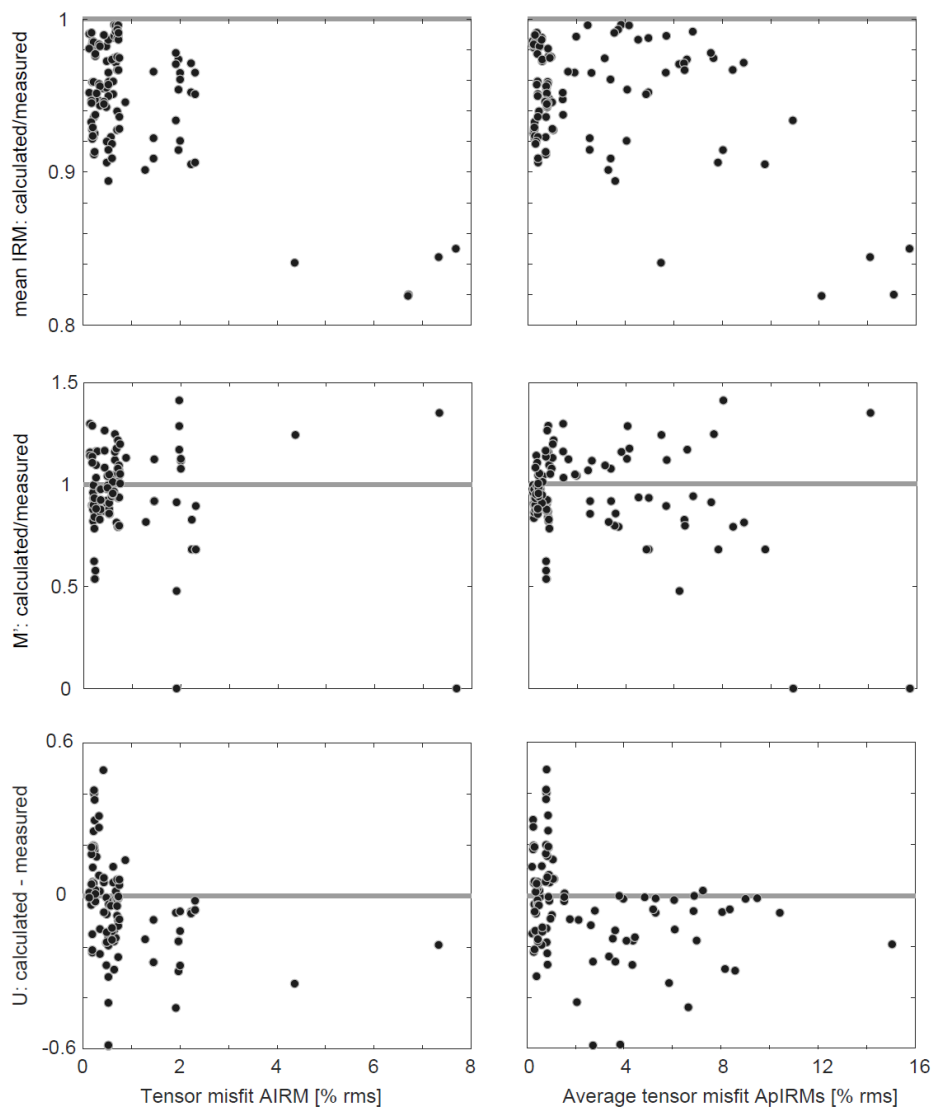


Figure 7: Deviations of measured and calculated AIRM parameters as a function of tensor misfit.